Magnetic Resonance Materials in Physics, Biology and Medicine (2022) 35:345–347
https://doi.org/10.1007/s10334-022-01015-5

COMMENTARY

Can detonation nanodiamonds serve as MRI phantoms?

Alexander M. Panich[1]

Received: 7 March 2022 / Revised: 18 April 2022 / Accepted: 19 April 2022 / Published online: 26 April 2022

Magnetic resonance imaging (MRI) phantoms are routinely used for calibrating MRI machines and characterizing the MRI system performance, such as resonance frequency, spin–spin and spin–lattice relaxation times, signal-to-noise ratio, image uniformity, spatial resolution, and phase related image artifacts [1]. Phantoms should be non-toxic, stable, inexpensive, easy to use and desirably having relaxation times comparable to those of human tissues. Two types of MRI phantoms are commonly used: aqueous solutions and gels. The aqueous solutions of paramagnetic salts such as $CuSO_4$, $NiCl_2$, $MnCl_2$, or $GdCl_3$ exhibit homogeneous spin–lattice (T_1) and spin–spin (T_2) relaxation times throughout the phantom and long-term stability. Herewith, the liquid phantom needs some stabilization time before the measurement. Gel phantoms include agarose, agar, polyvinyl alcohol, gelatin, gelatin-agar, or some other medium with the addition of paramagnetic substances (usually $GdCl_3$) to adjust the relaxation time [2]. However, the aforementioned compounds are toxic [3–6], and their handling, shipping and disposal are questionable owing to possible contamination of the MRI equipment and personnel. Therefore, the scientific community continues to develop new phantoms that would be free of the aforementioned disadvantages and would validate the accuracy of the in vivo measurements, as well as repeatability and reproducibility of measurements across imaging platforms and time.

To this end, Sękowska et al. have recently reported on the eventual application of detonation diamond nanoparticles in phantoms for MRI [7]. The phantoms were produced using distilled water, agar (1.413%) and carrageenan (2%) with addition of the detonation nanodiamond (DND) particles of the average size of 4–5 nm suspended in dimethyl sulfoxide (DMSO) and treated by 5-min-long high-power ultrasound sonication. The content of the DND-DMSO suspension in prepared phantoms was set to 0%, 8%, 10% and 12%, respectively. The contents were thoroughly mixed, poured into molds and placed to congeal. Surprisingly, the authors obtained a linear dependence of the spin–lattice (T_1) and spin–spin (T_2) relaxation times of the phantoms on the nanodiamond concentration (See Figures 3 and 5 in ref [7].). This result contradicts our recent experimental nuclear magnetic resonance (NMR) data on DND suspensions [8–10], as well as some fundamentals of the relaxation phenomena in nuclear spin systems [11, 12].

Let us now analyze the nuclear relaxation data in our DND suspensions and discuss whether these compounds can be used as MRI phantoms. As it is well known, DND particles exhibit intrinsic localized paramagnetic defects: (i) P1 nitrogen paramagnetic defects distributed throughout the diamond core and (ii) unpaired electron spins of dangling bonds positioned mainly in the near-surface layer [13–15]. The overall defect density in the DND particles measured by EPR is around 6×10^{19} spin/g [13–15]. In DND suspensions, the relaxation of the proton nuclear spins of the solvent is accelerated owing to the interaction of protons with unpaired electron spins of the aforementioned paramagnetic defects [8–10]. The contributions of the DND-inherent paramagnetic defects to the experimentally measured proton spin–lattice and spin–spin relaxation rates R_1^{exp} and R_2^{exp} in suspensions are described by the second term of equations [8]

$$R_1^{exp} = \frac{1}{T_1^{exp}} = \frac{1}{T_1^{solv}} + \frac{1}{T_1^{DND}} = R_1^{solv} + r_1^{DND} \times C_{DND} \quad (1)$$

$$R_2^{exp} = \frac{1}{T_2^{exp}} = \frac{1}{T_2^{solv}} + \frac{1}{T_2^{DND}} = R_2^{solv} + r_2^{DND} \times C_{DND} \quad (2)$$

where T_1^{solv} and T_2^{solv} are the spin–lattice and spin–spin relaxation times of the solvent, T_1^{DND} and T_2^{DND} are the spin–lattice and spin–spin relaxation times caused by paramagnetic defects of the nanodiamond particles, C_{DND} is the concentration of DND particles in suspensions, and r_1 and r_2 are the relaxivities defined as the slopes of the concentration dependences of $\frac{1}{T_1^{exp}}$ and $\frac{1}{T_2^{exp}}$. Here T_1^{solv} and T_2^{solv} are the char-

✉ Alexander M. Panich
pan@bgu.ac.il

[1] Department of Physics, Ben-Gurion University of the Negev, 8410501 Beer-Sheva, Israel

acteristics of the specific liquid solvent used and, therefore, are constant for all measurements.

The results of our measurements of the spin–lattice and spin–spin relaxation times and rates of water protons in aqueous DND suspensions as a function of the DND concentration are shown in Figs. 1 and 2. The data show that the paramagnetic defects of the DND particles (i) affect the relaxation rates of protons in suspension and (ii) reveal linear dependence of the relaxation rates R_1^{DND} and R_2^{DND}(not relaxation times!) on the DND content, which is fully consistent with the fundamentals of the spin relaxation theory [11, 12], revealing a linear proportionality of the relaxation rate to the concentration of paramagnetic defects. This is a universal law, which is valid for liquids, gels, and solids (for example, see Reviews [14–16]). Herewith, as it follows from Eqs. 1 and 2 and the experimental data shown in Figs. 1 and 2, both proton spin–lattice and spin–spin relaxation times exhibit a hyperbolic dependence on the nanodiamond concentration C_{DND} in suspension:

$$T_1 = \frac{1}{R_1^{solv} + r_1^{DND} \times C_{DND}} \quad (3)$$

$$T_2 = \frac{1}{R_2^{solv} + r_2^{DND} \times C_{DND}} \quad (4)$$

These experimental results are in complete agreement with the published literature and the fundamentals of relaxation phenomena in nuclear spin systems. We note that similar hyperbolic-like concentration dependence of T_1 was recently obtained in measurements of the ^{1}H spin–lattice relaxation of aqueous solutions of nanodiamonds of 18 and 125 nm in diameter, prepared by the high pressure–high

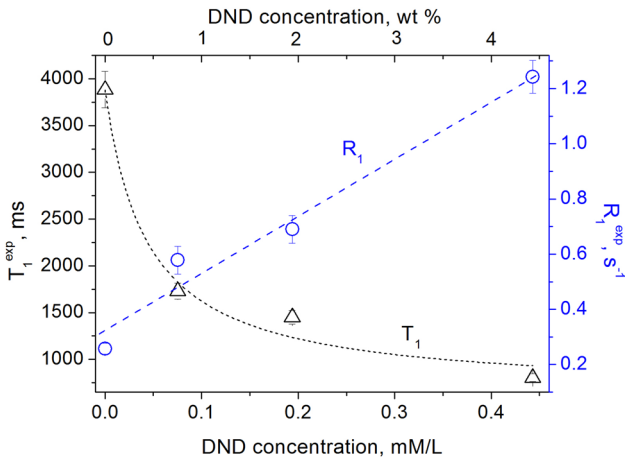

Fig. 1 Dependence of the spin–lattice relaxation rate R_1 and spin–lattice relaxation time T_1 of water protons in aqueous DND suspensions on the concentration of DND particles in suspensions

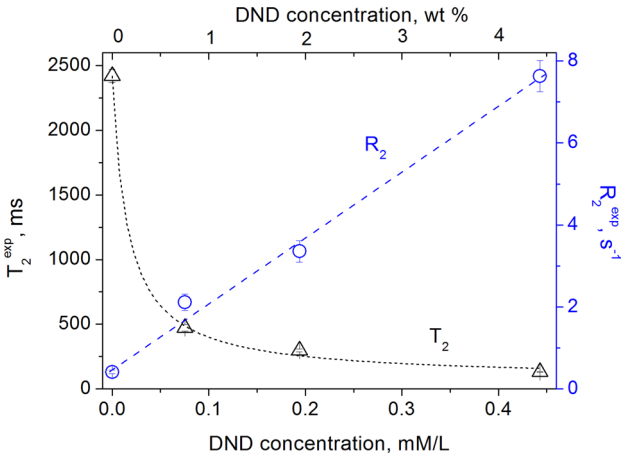

Fig. 2 Dependence of spin–spin relaxation rate R_2 and spin–spin relaxation time T_2 of water protons in aqueous DND suspensions on the concentration of DND particles in suspensions

temperature (HPT) technique [17]. These results support well my above findings.

Recently, Thangavel et al. [18] measured the relaxivities r_1 and r_2 in aqueous solutions of common paramagnetic agents ($CuSO_4$, $MnCl_2$, and $NiCl_2$) at room temperature and a magnetic field of 3 T. Separate phantoms were prepared at various concentrations from 0.05 to 0.5 mM for $MnCl_2$ and from 1 to 6 mM for $CuSO_4$ and $NiCl_2$, and were reported to reveal relaxivities $r_1 = 0.602$ mM^{-1} s^{-1} and $r_2 = 0.730$ mM^{-1} s^{-1} for $CuSO_4$, $r_1 = 6.397$ mM^{-1} s^{-1} and $r_2 = 108.266$ mM^{-1} s^{-1} for $MnCl_2$, $r_1 = 0.620$ mM^{-1} s^{-1} and $r_2 = 0.848$ mM^{-1} s^{-1} for $NiCl_2$ (Table 1). Our nanodiamond suspensions showed relaxivities $r_1 = 2.1$ mM^{-1} s^{-1} and $r_2 = 15.8$ mM^{-1} s^{-1} in $B_0 = 8$ T [8], which are higher than those of $CuSO_4$ and $NiCl_2$ and lower than that of $MnCl_2$. We note that our measurements were done in in $B_0 = 8$ T, and since r_1 and r_2 increase with decreasing magnetic field [19], we expect that the DND suspensions will show several times higher relaxivities in magnetic fields from 1 to 3 T used in clinical MRI scanners.

In conclusion, we also note that the amount of paramagnetic defects in DND can be increased by irradiation [20], which would lead to higher relaxivities. Herewith the relaxation time $T_1 = 805$ ms for a DND concentration of 4.64 mM in our suspension coincides with the relaxation time of the

Table 1 Relaxivities r_1 and r_2 of several MRI phantoms

Compound	r_1, mM^{-1} s^{-1}	r_2, mM^{-1} s^{-1}	Magnetic field	Reference
$CuSO_4$	0.602	0.730	3 T	[18]
$NiCl_2$	0.620	0.848	3 T	[18]
$MnCl_2$	6.397	108.266	3 T	[18]
DND	2.1	15.8	8 T	[8]

human tissue $T_1 = 810.5$ ms [7]. It is important that the DND suspensions are non-toxic, very stable and do not undergo noticeable changes and precipitation during several years of storage. They are robustly processed, safe, readily available, inexpensive and easy to handle. Therefore, summarizing all of the above, nanodiamonds can be considered suitable for use as MRI phantoms.

Acknowledgements We thank Dr. Moti Salti (Brain Imaging Research Center, Ben-Gurion University of the Negev) for useful discussion.

References

1. Keenan KE, Ainslie M, Barker AJ, Boss MA, Cecil KM, Charles C et al (2018) Quantitative magnetic resonance imaging phantoms: A review and the need for a system phantom. Magn Reson Med 79:48–61
2. Hattori K, Ikemoto Y, Takao W, Ohno S, Harimoto T, Kanazawa S, Oita M, Shibuya K, Kuroda M, Katoa H (2013) Development of MRI phantom equivalent to human tissues for 3.0-T MRI. Med. Phys. 40:032303
3. Spencer AJ, Wilson SA, Batchelor J, Reid A, Rees J, Harpur E (1997) Gadolinium chloride toxicity in the rat. Toxicol Pathol 25:245–255
4. Stannard L, Doak SH, Doherty A, Jenkins GJ (2017) Is nickel chloride really a non-genotoxic carcinogen? Basic Clin Pharmacol Toxicol 121:10–15
5. Sepúlveda MR, Dresselaersc T, Vangheluwe P, Everaerts W, Himmelreich U, Mata AM, Wuytack F (2012) Evaluation of manganese uptake and toxicity in mouse brain during continuous $MnCl_2$ administration using osmotic pumps. Contrast Media Mol Imaging 7:426–434
6. TOXNET. 1975–1986. National library of medicine's toxicology data network. Hazardous Substances Data Bank (HSDB). Public Health Service. National Institute of Health, U.S. Department of Health and Human Services. Bethesda, MD: NLM
7. Sękowska A, Majchrowicz D, Sabisz A, Ficek M, Bułło-Piontecka B, Kosowska M et al (2020) Nanodiamond phantoms mimicking human liver: perspective to calibration of T_1 relaxation time in magnetic resonance imaging. Sci Rep 10:6446–6452
8. Panich AM, Salti M, Goren SD, Yudina EB, Aleksenskii AE, Vul' AYa, Shames AI, (2019) Gd(III)-grafted detonation nanodiamonds for MRI contrast enhancement. J Phys Chem C 123:2627–2631
9. Panich AM, Shames AI, Goren SD, Yudina EB, Aleksenskii AE, Vul' AYa, (2020) Examining relaxivities in suspensions of nanodiamonds grafted by magnetic entities – comparison of two approaches. Magn Reson Mater Phys Biol Med (MAGMA) 33:885–888
10. Panich AM, Salti M, Prager O, Swissa E, Kulvelis YV, Yudina EB, Aleksenskii AE, Goren SD, Vul AY, Shames AI (2021) PVP-coated Gd-grafted nanodiamonds as a novel and potentially safer contrast agent for in-vivo MRI. Magn Reson Med 86:935–942
11. Abragam A (1961) The Principles of Nuclear Magnetism. Clarendon Press, Oxford, U.K.
12. Bloembergen N (1957) Proton relaxation times in paramagnetic solutions. J Chem Phys 27:572–573
13. Shames AI, Panich AM, Kempiński W, Alexenskii AE, Baidakova MV, Dideikin AT, Osipov VYu, Siklitski VI, Osawa E, Ozawa M, Vul AY (2002) Defects and impurities in nanodiamonds: EPR, NMR and TEM study. J Phys Chem Solids 63:1993–2001
14. Shames AI, Panich AM (2017) Paramagnetic defects in nanodiamonds. In: Arnault JC (Ed) Nanodiamonds: Advanced Material Analysis, Properties and Applications. Elsevier, Ch. 6, pp 131–154
15. Panich AM (2012) Nuclear magnetic resonance studies of nanodiamonds. Crit Rev Solid State Mater Sci 37:276–303
16. Panich AM (2017) Nuclear magnetic resonance studies of nanodiamond surface modification. Diamond Relat Mater 79:21–31
17. Waddington DEJ (2018) Diamonds on the inside: imaging nanodiamonds with hyperpolarized MRI. PhD Thesis. The University of Sydney. https://ses.library.usyd.edu.au/handle/2123/17948
18. Thangavel K, Saritas EU (2017) Aqueous paramagnetic solutions for MRI phantoms at 3 T: A detailed study on relaxivities. Turk J Elec Engin Comp Sci 25:2108–2121
19. Bertini I, Luchinat C, Parigi G, Ravera E (2015) NMR of Paramagnetic Molecules: Applications to Metallobiomolecules and Models, 2nd edn. Elsevier, Amsterdam
20. Shenderova OA, Shames AI, Nunn NA, Torelli MD, Vlasov I, Zaitsev A (2019) Review Article: Synthesis, properties, and applications of fluorescent diamond particles. J Vacuum Sci Techn B 37:030802